This is a pre print version of the following article:

Design of an Additive Manufactured Steel Piston for a High Performance Engine: Developing of a Numerical Methodology Based on Topology Optimization Techniques / Barbieri, S. G.; Giacopini, M.; Mangeruga, V.; Mantovani, S.. - In: SAE TECHNICAL PAPER. - ISSN 0148-7191. - 2018-:6(2018), pp. 1139-1150. (Intervento presentato al convegno 2018 SAE World Congress Experience, WCX 2018 tenutosi a Cobo Center, usa nel 2018) [10.4271/2018-01-1385].

Terms of use:

The terms and conditions for the reuse of this version of the manuscript are specified in the publishing policy. For all terms of use and more information see the publisher's website.

25/04/2024 18:06

(Article begins on next page)

SAE International Journal of Engines

Design of an additive manufactured steel piston for a high performance engine: developing of a numerical methodology based on topology optimization techniques

--Manuscript Draft--

Manuscript Number:	JENG-2018-0025R1
Full Title:	Design of an additive manufactured steel piston for a high performance engine: developing of a numerical methodology based on topology optimization techniques
Short Title:	Topology optimization of an additive manufactured steel piston
Article Type:	Review Paper
Corresponding Author:	Saverio Giulio Barbieri ITALY
Corresponding Author Secondary Information:	
Corresponding Author's Institution:	
Corresponding Author's Secondary Institution:	
First Author:	Saverio Giulio Barbieri
First Author Secondary Information:	
Order of Authors:	Saverio Giulio Barbieri
	Matteo Giacopini, PhD
	Valerio Mangeruga
	Sara Mantovani, PhD
Additional Information:	
Question	**Response**
Have you submitted this paper to another publication with SAE or elsewhere?	Yes
Please give full details below as follow-up to "Have you submitted this paper to another publication with SAE or elsewhere?"	Paper already accepted for WCX World Congress Experience (2018-01-1385). Total weighted score received of 88.333333333 and invited for journal consideration.
Would you like to have author contact information included at the end of your manuscript?	Yes - Yes, I would like to provide contact information to be added at the end of my manuscript if it is accepted for publication
Please indicate the contact information exactly as you would like it to appear on your manuscript if it is accepted and published. as follow-up to "Would you like to have author contact information included at the end of your manuscript?"	Saverio Giulio Barbieri, University of Modena and Reggio Emilia, Engineering Department "Enzo Ferrari", Via Vivarelli 10, 41125, Modena, Italy, email:saveriogiulio.barbieri@unimore.it
For the purpose of a blinded review, please ensure that all contact and identifying information is removed from your manuscript prior to submitting your paper, including on the first page, any contact information on the last page, as well as any identifying information in the file name.	I have removed all contact and identifying information from my manuscript

Powered by Editorial Manager® and ProduXion Manager® from Aries Systems Corporation

Assignor represents, warrants and guarantees that (1) the Work is an original unpublished work; (2) Assignor is the sole and exclusive owner and claimant of all right, title and interest in and to the Work, including all copyrights therein, and neither the Work nor copyrights have been assigned, transferred or otherwise encumbered; (3) the Work contains no material whose publication would violate any copyright or other personal or proprietary right of any person or entity; (4) the Work is not a work made for the United States Government; and (5) Assignor has the authority to transfer the rights to Assignee and cause this Agreement to be executed as of the date first written above. Assignor further represents, warrants and guarantees, to the best of Assignor's knowledge and ability, that the Work is NOT controlled for export from the United States to any non-U.S. person or any other nation under the International Traffic in Arms Regulations (22 CFR Parts 120–130) or the Export Administration Regulations (15 CFR Parts 730–774) and, accordingly, may be modified, used, copied, distributed or circulated by SAE, in whole or in part, without any export licenses under the foregoing regulations. Assignor hereby assigns to SAE all right, title and interest in and to Assignor's copyright in the Work in the exclusive rights: (1) to reproduce the Work in all media now known or hereinafter devised; (2) to distribute copies of the Work in all media now known or hereinafter devised; and (3) to prepare derivative works based upon the Work including, for example, but not limited to, the right with respect to all or part of the Work to edit, annotate, comment, format/reformat and abstract the Work or incorporate it into a compilation, collection or other work. No other exclusive rights in the Work are hereby assigned. Assignor agrees that it shall not dispute, contest, or aid or assist others in disputing or contesting, either directly or indirectly, SAE's exclusive right, title and interest in the Work and in any and all compilations, collective works and derivative works based on the Work, including copyrights therein or other proprietary rights therein claimed by SAE. Assignor agrees that, for no additional compensation, Assignor will execute any and all documents that may be necessary to assist SAE to register, perfect and	Copyright Assigned to SAE International

enforce SAE's rights in and to the Work and any and all compilations, collective works and derivative works based on the Work. SAE hereby grants Assignor the nonexclusive right to reproduce and publicly distribute the Work in electronic/optical media following six (6) months after first publication by SAE. Any such reproduction or distribution of the Work shall include the SAE copyright notice thereon and shall not be offered for sale or used to imply endorsement by SAE of a service or product. The Assignor may also post an electronic version of the accepted Work to an institutional repository, but not the final typeset Work. Nothing herein shall prohibit Assignor's reproduction and noncommercial distribution of the Work for its own use. Use by Government Employees or Papers Published Under Government Contract:	
Select one of the options related to copyright release above.	I am authorized to represent my fellow authors of the above-listed paper in assigning copyright.
Order of Authors Secondary Information:	

Reviewer: #1
The authors thank the referee for his careful, constructive review and for his suggestions. The paper has been amended according to the reviewer's suggestions, and the authors feel that the present version is better and clearer.
The points raised by the reviewer are separately examined in the following.

Overall a good publication, with good science, and a novel topic.

1) From a combustion perspective, examining piston @TDC in the combustion stroke would not represent peak pressure conditions. Normally maximum pressure should be circa 5-10deg ATDC, depending on speed/load. Regardless, I do not suggest you alter the publication, merely take this into account in further work.

Actually the maximum chamber pressure (12 crank angle degrees after TDC) has been used. The authors decided to neglect the corresponding conrod tilting in order to not include in this load case the piston/liner contact interaction. The following sentence has been added at page 3 of the text:

"Actually, these values have been recorded at the instant of maximum combustion pressure, which is located approximately 12 crank angle degrees after top dead centre. The connecting rod should be lightly tilted, but the authors preferred to keep it perfectly vertical to not complicate the model with the piston-liner contact interaction. Thrust forces related to the piston-liner interaction are then considered in a different specific optimization load case."

2) For the 1D model validation, the model of the spark plug pressure sensor would be helpful. Also note for future reference you may have had superior correlation if you used a pressure sampling rate of 0.5 to 0.2 CAD; 1.0 CAD is acceptable but considered bordering on too low resolution to be meaningfully accurate.

The authors perfectly agree with this reviewer. Indeed, the 1° crank angle (re)sapling has been adopted only for load estimation in the mechanical analysis. A finer resolution has been adopted in 1-D cfd analysis which are out of the scope of the present contribution. The following sentence has been modified in the text at page 3:

"Both the acceleration and the gas pressure were resampled in 1° crankshaft angle steps for the structural analysis, and the corresponding values were employed for the different piston positions considered."

3) You propose the peak temperature of the piston was simulated to be 280C, in my experience this is very high, and may be beyond the material capability of a stock Al piston. Without any information to correlate this as reasonable it puts the validation of the model into question: If the engine could not sustain the temperature the CFD is claiming, then the model may not be representative.

The authors perfectly agree with this review. The following sentence has been added in section Thermal analysis and reference [16] has been also included:

"Actually, an experimental campaign in order to validate the thermal model has not been performed for the specific engine under investigation. Nevertheless, the methodology employed

by the authors has been previously validated in [16] versus experimental evidences for a similar engine thus increasing confidence on the numerical forecasts obtained."

4) The engine conditions would also helpful; I assume we are referring to peak power, but note that for force analysis peak torque or peak BMEP could be higher that at TDCC. Adding a table with engine speed/load validated against would be ideal, as well as a table with what kind of engine we are talking about; the introduction mentions forced induction, but the authors do not clarify engine capacity, swept volume, bore'stroke ratio, power rating, induction type, compression ratio, piston-to-bore clearance, bore liner treatment/surface, or after-treatment classification. We do not even know if we are discussing a passenger car engine, and all of these characteristics would add value to the publication, and help place the relevance of this technique in the realm of possible engine technologies.

Details about the engine have been added at the end of section "Introduction", page 1.

5) All CFD software output Figures need reasonable scales, and readable font sizes. Fig.8 in particular is exceptionally bad; it is nearly impossible to read the tiny 2.806e+002. It should be 280.6C, and in a font that is readable.

Corrected. Thanks.

6) Fig 24 & 27 are in too dark a colour to distinguish. A lighter colour than deep navy would help readability.

Corrected. Thanks.

7) On the discussion of piston temperature I am sceptical: We can not assume to know the cooling effect of a piston cooling jet with such a radical piston design; indeed, the understanding how the PCJ effect changes with this design would be the subject of a publication in its self. I do not believe it is reasonable to claim 60C temp drop by adding a 2nd PCJ as suggested in the thermal analysis without further qualifying the statement. It may absolutely be true, but there is no evidence to support the statement is offered. I propose the sentence changed to reflect "the temperature may be reduced further by adding a 2nd PCJ" if suitable correlating evidence can not be provided.

We have further improved the piston geometry and we have (re)run all the simulations. Now the steel piston thermal analysis is performed considering the same boundary conditions adopted for the aluminium piston thermal analysis. The section has been modified as follows:

"Thermal analysis

A thermal model has been prepared, based on the same boundary conditions of Table 4. In particular, the thermal exchange contribution given by the oil jet and the rest of the splashed oil has been considered to be exactly the same of the previously investigated aluminium piston.

Results

Figure 30 shows the temperature contour plot. The piston crown reaches a maximum temperature of 490°C.
In particular, these high values of temperature are confined to a small angular portion of the valve pocket peripheries, while the rest of the top surface exhibits a comparable temperature distribution with respect to the aluminium piston (ranging from 250°C to 290°C). Such a result has been obtained properly designing very thin geometrical features of the piston top (Figure 31), thus minimizing the thermal resistance through the piston top thickness. In fact, the thermal conductivity of steel can be up to five times lower than the aluminium one.

Unfortunately, it has not been possible to remove material under the identified critical portions of the valve pockets periphery without modifying the non-design space (Figure 32). A smoother temperature gradient could be obtained softening the geometry of these keen-edged features, but it will simultaneously increase the combustion chamber volume, thus reducing the compression ratio and the maximum power of the engine. Cooling galleries could be designed in order not to modify the geometry of the crown. Furthermore, an integrated in-cylinder/CHT analysis should be performed in order to guide the redesign process and to predict possible abnormal combustion occurrence related to these concentrated peaks of temperature [19]. ”

8) There is no discussion on the implication of a 550C temperature on the feasibility of the component; any surface significantly above 300C would make controllable combustion unlikely. With simulated temperatures of 550C the technical feasibility of this exercise (particularly given the 9% mass increase) make it a non-starter. This does not detract at all from the scientific interest of the paper, but in the interest of a rounded conclusion should be mentioned in the conclusion. As it presently stands, the Conclusion infers the main disadvantage of the proposal is the minor weight increase, which is inaccurate.

The authors perfectly agree with this review, these values of temperature need deeper CFD studies and a redesign process of the piston top to be performed. Thermal section and conclusions have been consequently modified.

Reviewer: #3

The authors thank the referee for his careful, constructive review and for his suggestions. The paper has been amended according to the reviewer's suggestions, and the authors feel that the present version is better and clearer.

The points raised by the reviewer are separately examined in the following.

Overall this is a very good paper. With high BMEP engines using EGR, high cylinder pressure is a current limitation. The traditional methods of increasing piston strength have been sub-optimal due to the increases in piston weight and component contribution to friction.

A few minor suggestions:

1) The details of the FEA model and material properties would read better as a table (Finite Element analysis of the aluminium piston - 2nd paragraph). Same comment for the Finite element validation section.

Tables added. Thanks.

2) Keep the scaling for the von Mises contour plots consistent for Fig 3,5,7. Helps easily show the stress difference between cases. Same comment for Fig 23,25,26.

Corrected. Thanks.

3) Clearly explain why the choice of relative density went from 0.4->0.5->0.4 in Fig 13,15,17.

The authors selected the particular lower bound of relative density contour plot in order to better highlight the structural features identified by each load case.

The text has been modified as follows:

"The results of the optimization process have been discussed in terms of relative density contour plots. Each load case has been analysed independently in order to better understand how the density distribution is influenced by the load path and by the design constraints. Different values of lower bound relative density, namely 0.1, 0.4 and 0.5 have been set to highlight the structural features proposed by the optimization analysis and let the reader clearly understand the consequent redesign process."

4) Add clarification language to captions of Fig 29,30 to include addition of second oil jet boundary condition in Fig 30.

We have further improved the piston geometry and we have (re)run all the simulations. Now the steel piston thermal analysis is performed considering the same boundary conditions adopted for the aluminium piston thermal analysis. The section has been modified as follows:

"Thermal analysis

A thermal model has been prepared, based on the same boundary conditions of Table 4. In particular, the thermal exchange contribution given by the oil jet and the rest of the splashed oil has been considered to be exactly the same of the previously investigated aluminium piston.

Results

Figure 30 shows the temperature contour plot. The piston crown reaches a maximum temperature of 490°C.

In particular, these high values of temperature are confined to a small angular portion of the valve pocket peripheries, while the rest of the top surface exhibits a comparable temperature distribution with respect to the aluminium piston (ranging from 250°C to 290°C). Such a result has been obtained properly designing very thin geometrical features of the piston top (Figure 31), thus minimizing the thermal resistance through the piston top thickness. In fact, the thermal conductivity of steel can be up to five times lower than the aluminium one. Unfortunately, it has not been possible to remove material under the identified critical portions of the valve pockets periphery without modifying the non-design space (Figure 32). A smoother temperature gradient could be obtained softening the geometry of these keen-edged features, but it will simultaneously increase the combustion chamber volume, thus reducing the compression ratio and the maximum power of the engine. Cooling galleries could be designed in order not to modify the geometry of the crown. Furthermore, an integrated in-cylinder/CHT analysis should be performed in order to guide the redesign process and to predict possible abnormal combustion occurrence related to these concentrated peaks of temperature [19]. ”

5) High surface temperature achieved with new design may result in increased knock. Address this in more detail with supporting literature to say if it will/will not be an issue.

The authors perfectly agree with this review, these values of temperature need deeper CFD studies and a redesign process of the piston top to be performed. Thermal section and conclusions have been consequently modified. Moreover reference [19] has been included.

Manuscript
Click here to download Manuscript
PISTON_SAE_journal_rev01.docx

Design of an additive manufactured steel piston for a high performance engine: developing of a numerical methodology based on topology optimization techniques

Abstract

Modern high performance engines are usually characterized by high power densities, which lead to high mechanical and thermal loadings acting on engine components. In this scenario, aluminium may not represent the best choice for piston manufacturing and steel may be considered as a valid alternative. In this paper, a methodology involving optimization techniques is presented for the design of an internal combustion engine piston. In particular, a design strategy is preliminary investigated aiming at replacing the standard aluminium piston, usually manufactured by forging or casting, with an alternative one made of steel and manufactured via an Additive Manufacturing process. Three different loading conditions are employed for the topology optimizations set up. Optimization results are then interpreted and the various structural features of the steel piston are designed starting from the density distribution contour plots. Different Finite Element thermo-mechanical models are finally prepared in order to correct and validate the designed geometry.

Introduction

The piston represents the main alternating mass in an internal combustion engine crank mechanism. To minimize piston mass is therefore fundamental to contain inertial forces. Because of its low density, aluminium is the material most commonly employed for piston manufacturing. Unfortunately, aluminium exhibits low mechanical properties, which further decrease when it is exposed to high temperatures [1]. Turbocharging (downsizing), high compression ratios, advanced spark ignitions strategies are some of the techniques employed in modern engines in order to increase engine efficiency to fulfil strict norms on engine pollution emissions and to minimize fuel consumption. As a consequence, higher specific loads are encountered which lead to higher mechanical and thermal loadings of engine components [2, 3]. In this scenario, aluminium may not represent the best choice and steel may be considered as a valid alternative for piston manufacturing. Schreer et al. [4] analysed the consequences of employing a steel piston: a better kinematic behaviour of the crank mechanism, a comparable weight, more homogeneous surface temperatures, a lower dead volume at the top land, a lower blow-by and a more efficient combustion process are the main advantages registered. Nevertheless, traditional manufacturing technologies cannot be employed when steel is considered as material for pistons. In fact, in order to obtain components with a comparable weight when compared with those made with aluminium, the thickness of the different parts of a steel piston have to be reduced up to one millimetre. Additive Manufacturing represents a promising technology to obtain thin features. Bendsøe and Kikuchi [5] related optimization techniques to structural design, noting that the resulting complex shapes could be easily reproduced by Additive Manufacturing. Du and Tao [6] and Zhao et al. [7] used the topology optimization for an engine piston lightening, but they used the results only to understand which parts of the piston were redundant, without ascribing any focused design validity. Brackett et al. [8] analysed the main challenges and opportunities for topology optimization for Additive Manufacturing. The importance of mesh resolution, manufacturing constraints and the post-processing have been highlighted.
In the present paper, the results of previous optimization analyses are interpreted [9]. In particular, three optimization load cases are considered and the different structural features of the piston are designed starting from each density distribution contour plot. Finite Element models are then prepared in order to validate the obtained geometry. Both thermal and structural analyses are performed.
Table 1 collects the main data of the engine equipped with the particular piston under investigation: it is a L-twin high performance four stroke engine for motorbike application.

Table 1. Engine data.

Engine configuration	L-twin
Displacement	955 cm^3
Bore	100 mm
Stroke	60.8 mm
Maximum power	157 HP @ 11000 rpm
Maximum torque	107 Nm @ 9000 rpm
Maximum combustion pressure	91 bar

Design Strategy

A design strategy is presented based on different subsequent steps:

1. *Finite Element analysis of the original aluminium piston*: first of all the original aluminium piston has been analysed. Structural simulations have been computed in order to record the displacements of some critical part of the component. In particular, at top dead centre during combustion and at top dead centre at the beginning of induction stroke, the displacement of particular nodes of the piston crown have been monitored. In the case of maximum piston thrust force, the nodes on the skirt in contact with the liner have been examined.
2. *Topology optimization of the steel piston*: the recorded displacements have been then employed in the topology optimization analysis as design constraints (maximum displacement allowed). Relative density distribution contour plots have been computed. These preliminary results have been debated in detail in Barbieri et al. [9] and they will be briefly presented in the next section for the sake of clarity.
3. *Steel piston design*: the topology optimization results have been interpreted and the different structural features have been identified, thus allowing a first proposal of the new steel piston to be designed.

4. *Finite Element validation*: Finite Element models, quite similar to the ones employed for analysing the original aluminium piston, have been set up in order to validate the new component. This process of design and validation has been repeated until a suitable piston geometry has been obtained.

Table 2 and 3 collect the main material properties employed to set up the numerical analyses.
It could seem wrong to use the properties of bulk isotropic materials, because Additive Manufacturing techniques always produce anisotropic components due to their lay-up style process. Nevertheless, results reported in the pertinent literature show that this assumption can be accepted, at least in the preliminary initial phase of the components design, with a negligible influence on the outcomes. Tolosa et al. [10] and Spierings et al. [11] performed static and fatigue tests respectively. They obtained selective laser molten steel with properties very close to the ones of the classic bulk material, even if a slightly anisotropic behavior was always reported. Kruth et al. [12] studied the scanning strategies of Selective Laser Melting techniques. A thin wireframe structure, similar to the one typically resulting from optimization calculations, requires a short scan vector. Hence, adjacent tracks are scanned rapidly one after the other, leaving little cool down time in between, thus resulting in high temperatures. Consequently, suitable wetting conditions are present leading to a high density of the material. Kahlen and Kar [13] determined the yield and ultimate strength of laser-fabricated parts. The interface of two consecutive layers is not found to be the weakest joint. However, the maximum strength is found to occur in a direction, which is inclined at an angle with the direction of material deposition. This angle is influenced by the temperature gradient during the solidification of the melt pool. Gardan et al. [14] presented a numerical optimization method for improving the internal structure of models produced by additive manufacturing. They developed a system to manage the additive manufacturing process and the material characterization for a better integration with the topological optimization technique.

Finite Element analysis of the aluminium piston

The original aluminium piston has been analysed. Structural simulations have been computed in order to record the displacements of some critical part of the component.
In particular, three different load cases have been taken into account:

1. top dead centre during combustion (*TDCC*)
2. top dead centre at the beginning of induction stroke (*TDCI*)
3. instant of maximum piston thrust force (*PT*)

The software employed is Marc2013.1. The components involved in the crank mechanism (piston, piston pin and the connecting rod small end) have been discretized and a symmetry plane has been properly adopted. Figure 2 shows the model employed to mimic the TDCC and TDCI conditions. Figure 3 shows the model employed to mimic the maximum piston thrust force condition. In this case, the connecting rod has been correctly tilted and a rigid surface has been introduced in order to simulate the cylinder liner reaction. About 620 thousand elements have been employed: 73 thousand pentahedral elements (bilinear, 6 nodes, 6 Gaussian integration points), 47 thousand hexahedral elements (bilinear, 8 nodes, 8 Gaussian integration points) and 500 thousand tetrahedral elements (first order, 4 nodes, one Gaussian integration points), the average element size being 1 millimetre. The material considered for the modelling of the connecting rod and of the piston pin is a generic steel, Table 2. The material considered for the modelling of the piston is a generic aluminium, Table 3.

Table 2. Steel data.

Young modulus	210000MPa
Density	7.8 kg/dm^3
Poisson's ratio	0.3
Thermal conductivity	0.039 W/mmK

Table 3. Aluminium data.

Young modulus	70000MPa
Density	2.7 kg/dm^3
Poisson's ratio	0.3
Thermal conductivity	0.17 W/mmK

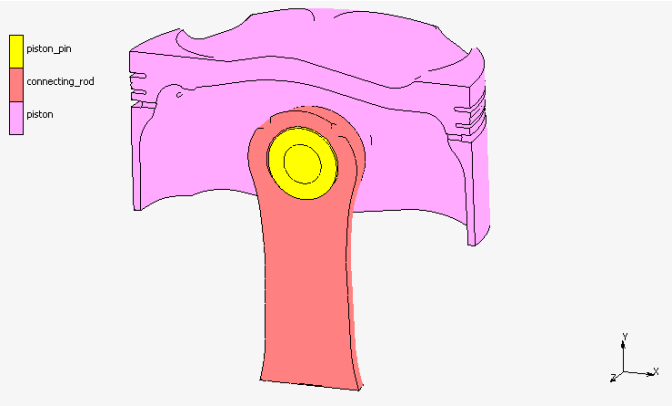

Figure 2. FE model used in the load cases of TDCC and TDCI.

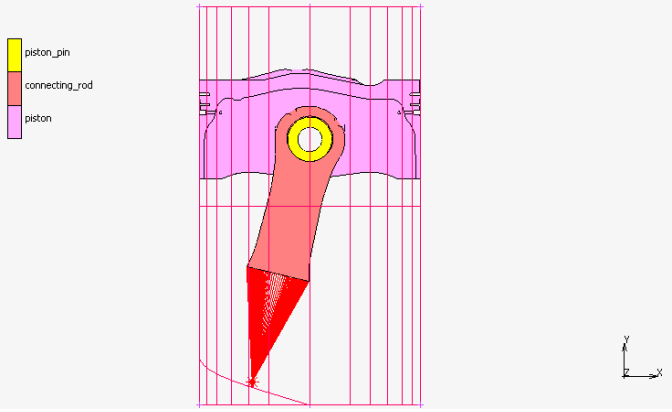

Figure 3. FE model used in the load cases of PT.

Structural analysis

A static model has been set up for each load case.
Different mechanical loads were applied depending on the piston position during the operating cycle. In particular, the alternating inertial acceleration was evaluated as a function of the crank angle θ by the classical formula

$$a(\theta) = \omega^2 r[cos\theta + \lambda \cos(2\theta)] \quad (1)$$

where ω is the angular velocity, r is the crank radius and λ is the connecting rod ratio. The inertial acceleration was applied to all the elements of the model, considering that the portion of connecting rod that was modelled approximately corresponds to its reciprocating part. The maximum power revving speed (Table 1) has been taken into account. It has been considered to be a good representation of the most severe working condition since maximum temperatures are registered together with high inertial loads and high combustion pressures. Actually, the maximum compressive forces are usually registered at maximum torque regime while maximum tensile inertial forces occur at maximum revving speed regime. Nevertheless, the authors decided to adopt the same operating condition for the different considered load cases (TDCC, TDCI and PT). In fact, the optimization process is based on a comparison between the mechanical behaviour of the original aluminium piston with the one observed considering the optimized steel piston. Consequently, it is not crucial to precisely identify the most severe loadings to be employed for each load case, but it is important that both the piston configurations (aluminium and steel) are analysed referring to the same (representative) operating conditions.
The combustion gas pressure, which acts on the top surface of the piston, was evaluated via a CFD one-dimensional model of the whole engine and validated versus the experimental data obtained during bench tests of the engine equipped with a spark plug combustion pressure sensor. Both the acceleration and the gas pressure were resampled in 1° crankshaft angle steps for the structural analysis, and the corresponding values were employed for the different piston positions considered.

Top dead centre during combustion (TDCC)

At TDCC a pressure of about 9.1 MPa has been applied on the piston top and a gravity load of 48769 m/s^2 has been assigned to the whole crank mechanism. Actually, these values have been recorded at the instant of maximum combustion pressure, which is located approximately 12 crank angle degrees after top dead centre. The connecting rod should be lightly tilted, but the authors preferred to keep it perfectly vertical to not complicate the model with the piston-liner contact interaction. Thrust forces related to the piston-liner interaction are then considered in a different specific optimization load case.
Figure 4 displays the von Mises stress contour plot. A maximum value of 92 MPa is registered under the piston top. The y-direction displacement of the nodes belonging to the piston top and lying on the symmetry plane has been recorded, Figure 5 a) and b).

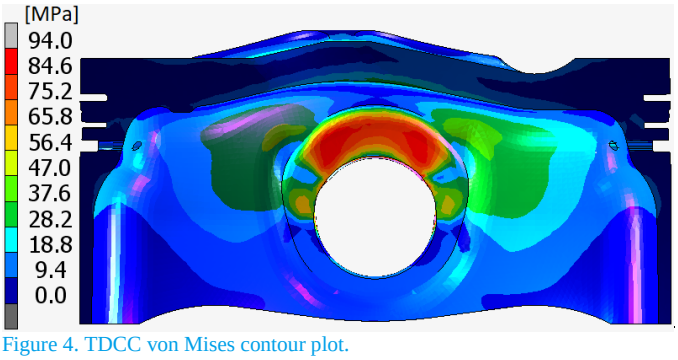

Figure 4. TDCC von Mises contour plot.

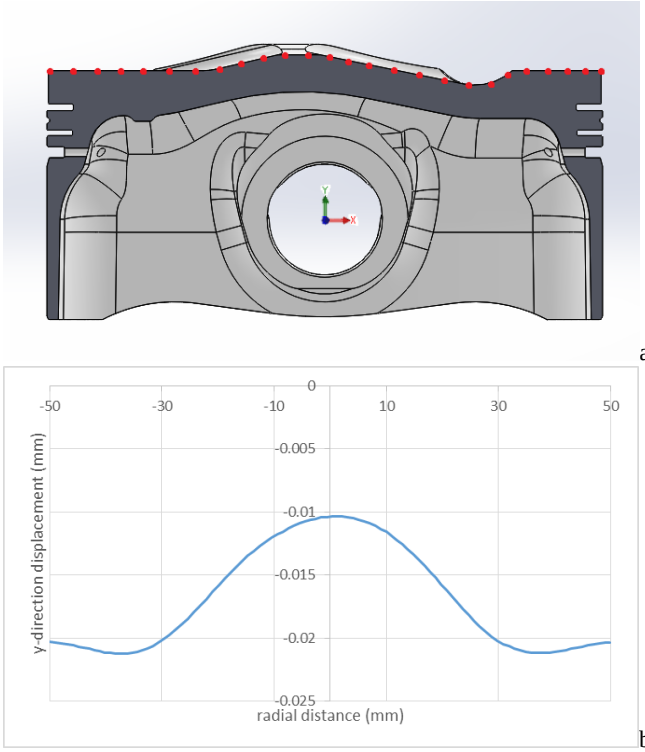

Figure 5. a) Nodes selected for design constraints; b) Y-direction displacement of the piston top at TDCC.

Top dead centre at the beginning of induction stroke (TDCI)

At TDCI a pressure of about 0.07 MPa has been applied on the piston top and a gravity load of 56008 m/s^2 has been assigned to the whole crank mechanism. Figure 6 displays the von Mises stress contour plot. A maximum value of 83 MPa is registered under the pin bosses. The y-direction displacement of the nodes belonging to the piston top and lying on the symmetry plane has been recorded, Figure 7.

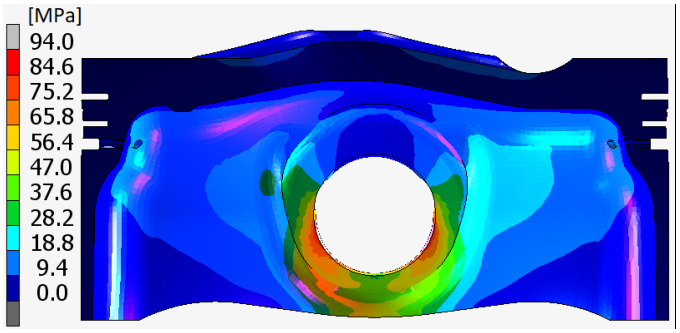

Figure 6. TDCI von Mises contour plot.

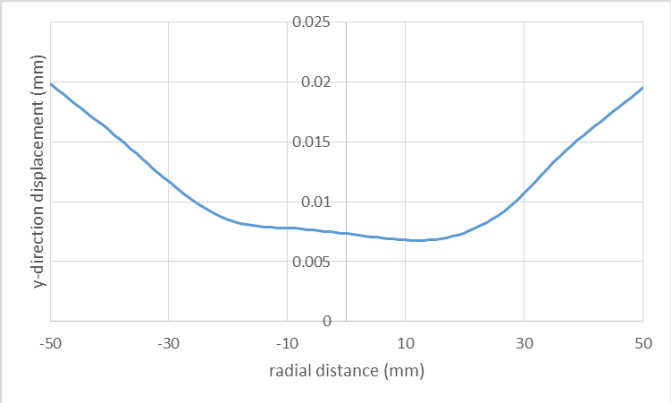

Figure 7. Y-direction displacement of the piston top at TDCI.

Maximum piston thrust force (PT)

At PT a pressure of about 0.8 MPa has been applied on the piston top and a negative gravity load of 22955 m/s^2 has been assigned to the whole crank mechanism. In this load case, the contact interaction between the piston and the liner is crucial. Figure 8 displays the von Mises stress contour plot. A maximum value of 93 MPa is registered near the skirt. The x-direction displacement of the nodes belonging to the skirt and in contact with the liner has been recorded.

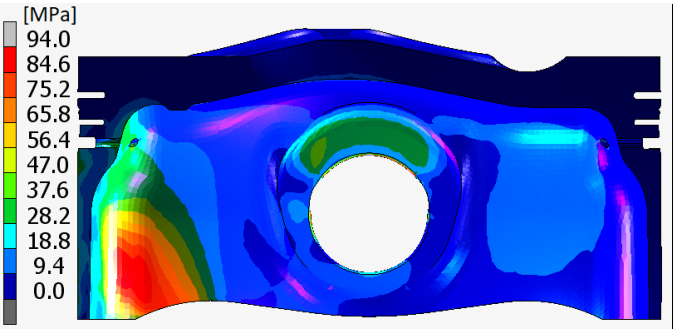

Figure 8. PT von Mises contour plot.

Thermal analysis

A static thermal analysis of the assembly has been prepared. Woschni [15] model has been employed for the calculation of the heat transfer coefficient and gas temperature to be applied on the piston top. All the other thermal boundary conditions, Table 4, have been calculated following the methodology presented in [1] and [16] at which the interest reader is referred. Actually, an experimental campaign in order to validate the thermal model has not been performed for the specific engine under investigation. Nevertheless, the methodology employed by the authors has been previously validated in [16] versus experimental evidences for a similar engine thus increasing confidence on the numerical forecasts obtained.

Table 4. Thermal boundary conditions.

Crown heat transfer coefficient	0.000637497 W/mm^2°C @1144°C
1st piston ring heat transfer coefficient	0.003812 W/mm^2°C @90°C
1st piston ring heat flux	0.104727 W/mm^2
2nd piston ring heat transfer coefficient	0.002344 W/mm^2°C @90°C
2nd piston ring heat transfer coefficient	0.104727 W/mm^2
Induction side skirt heat transfer coefficient	0.008834 W/mm^2°C @90°C
Induction side skirt heat flux	0.185425 W/mm^2
Exhaust side skirt heat transfer coefficient	0.008834 W/mm^2°C @90°C
Exhaust side skirt heat flux	0.283754 W/mm^2
Oil jet	0.005320 W/mm^2°C @120°C
Inner surfaces	0.0007734 W/mm^2°C @120°C
Outer surfaces	0.0015468 W/mm^2°C @120°C
Surfaces of piston pin and connecting rod	0.0005 W/mm^2°C @120°C

Results

Figure 9 shows the temperature contour plot. The piston crown reaches a maximum temperature of 280°C.

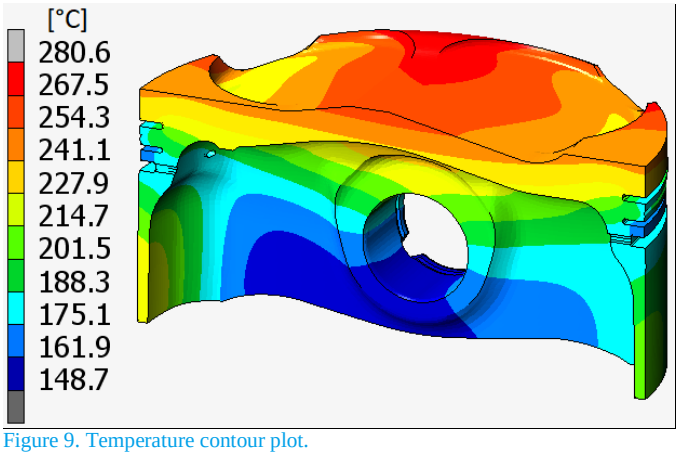

Figure 9. Temperature contour plot.

Topology optimization

In the following, an excerpt from [9] is reported, showing the topology optimization results.
The objective of the optimization is the minimization of the mass of the steel piston while keeping the same stiffness of the aluminum one.
Several optimization constraints have been imposed, based on the deformations registered with Finite Element analyses of the original aluminium piston briefly presented in the previous section.

Topology optimization process

The software package employed for the optimization is Altair OptiStruct 13, while the model set up has been made with Altair HyperMesh 13. In order to better calibrate the process, a sensitivity analysis on the optimization parameters DISCRETE (corresponding to the penalty factor, *p*) and MINDIM (related sensitivity filter, *r*) has been performed [9]. The choice of the parameters has been driven by the following considerations:

1. the solution achieved is more clearly defined;
2. the number of intermediate density elements is lower;
3. the convergence is achieved more easily;
4. the topology of the piston is considered more interesting, innovative, and easier to be manufactured by the designer;

After the sensitivity analysis, it has been chosen to set the optimization parameters to DISCRETE=3 and MINDIM=2.
The DISCRETE parameter influences the tendency for elements in a

topology optimization to converge to a material density of 0 or 1. Low values of this parameter help the solution to converge but results could be too sparse in terms of density distribution. Figure 10 shows the results for top dead centre during combustion. Only the elements with a relative density higher than 0.1 are shown. In this preliminary analysis a DISCRETE value of 1 has been set. The structural features are not easy to be interpreted and some elements are detached from the rest of the structure even a low relative density value is considered (see highlighted region in Figure 10).

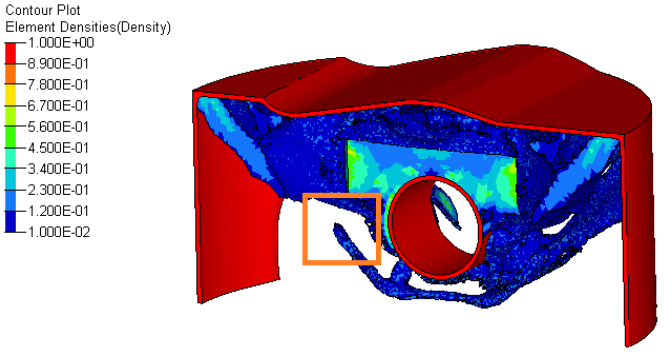

Figure 10. Contour plot TDCC 0.1 density, DISCRETE=1.

The MINDIM parameter specifies the minimum diameter of members formed in a topology optimization. A minimum dimension of 2 millimetres for each features of the steel piston has been chosen with the prospective to employ Additive Manufacturing as a manufacturing technique. Unnecessary high values of the MINDIM parameter could lead to suboptimal solutions. Figure 11 shows the results for top dead centre during combustion. Only the elements with a relative density higher than 0.1 are shown. In this preliminary analysis a MINDIM value of 4 has been set. This parameter forces the solver to converge to a low material density solution, which cannot lead to an easily interpretable result. Useful topology optimization results should display structural features at high values of relative density.

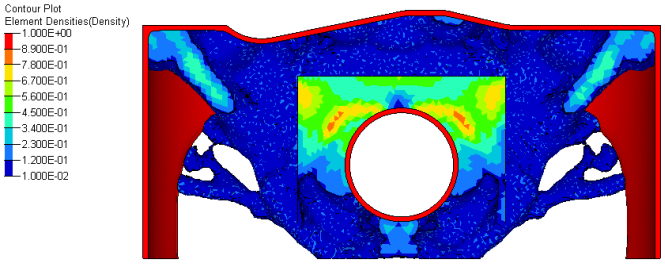

Figure 11. Contour plot TDCC 0.1 density, MINDIM=4.

Moreover, also the choice of the constrains has a crucial role in the model set up. For instance, Figure 12 shows the results for top dead centre at the beginning of induction stroke condition. In this analysis the constraints in terms of fixed displacements have been applied to the nodes of the upper side of the piston bosses. Only the elements with a relative density higher than 0.1 are shown. Results do not allow the structure to be interpreted since only a small portion of the design space is interested by the optimization process. In order to obtain good results, different constrains have to be adopted.

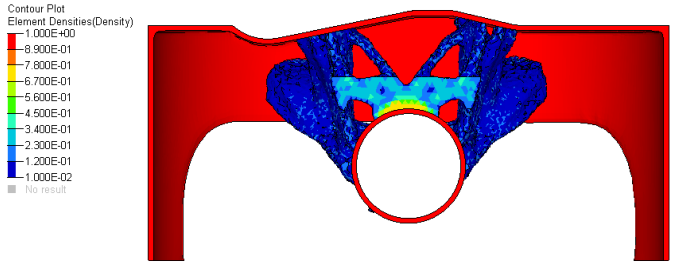

Figure 12. Contour plot TDCI 0.1 density, different constraints.

Topology optimization results

The results of the optimization process have been discussed in terms of relative density contour plots. Each load case has been analysed independently in order to better understand how the density distribution is influenced by the load path and by the design constraints. Different values of lower bound relative density, namely 0.1, 0.4 and 0.5 have been set to highlight the structural features proposed by the optimization analysis and let the reader clearly understand the consequent redesign process.
Figure 13 shows the results for top dead centre during combustion phase condition. It displays only the elements with a relative density higher than 0.1. Ribs linking the pin boss to the crown are visible. Moreover, a wireframe structure is present in the area below the pin boss, where the presence of high-density elements far from the crown increases the global bending stiffness of the piston. Increasing the lower bound of the relative density up to 0.4, Figure 14, supports that are fundamental for the stiffness of the piston are clearly identified.

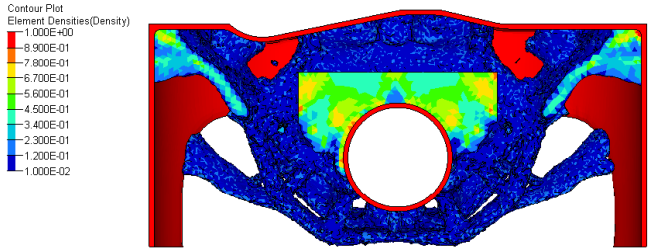

Figure 13. Contour plot TDCC 0.1 density.

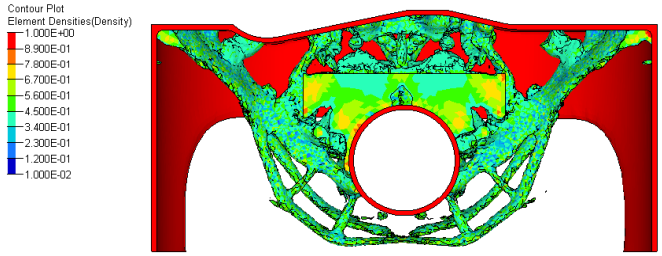

Figure 14. Contour plot TDCC 0.4 density.

Figure 15 shows the results for top dead centre at the beginning of induction stroke condition. Only the elements with a relative density higher than 0.1 are shown. Ribs linking the pin boss to the crown are visible. Moreover, a wireframe structure is present in the area below the pin boss, where the presence of high-density elements far from the crown increases the global bending stiffness of the piston. Increasing the lower bound of the relative density up to 0.5, Figure 16, supports that are fundamental for the stiffness of the piston are clearly identified.

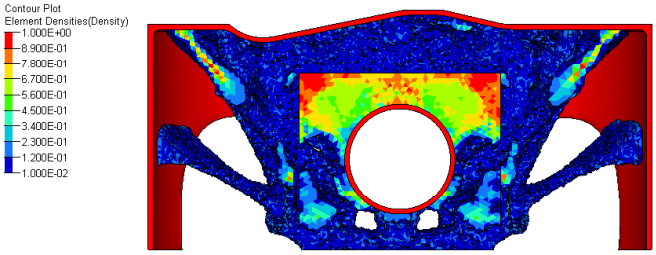

Figure 15. Contour plot TDCI 0.1 density.

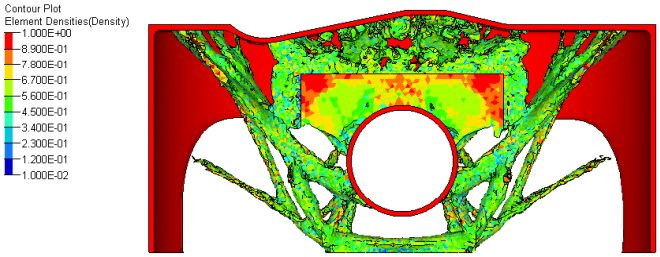

Figure 16. Contour plot TDCI 0.5 density.

Figure 17 shows the results for the maximum piston thrust force condition. Only the elements with a relative density higher than 0.1 are displayed. Ribs linking the pin boss to the skirt are visible. Increasing the lower bound of the relative density up to 0.4, Figure 18, supports that are fundamental for the stiffness of the piston are clearly identified.

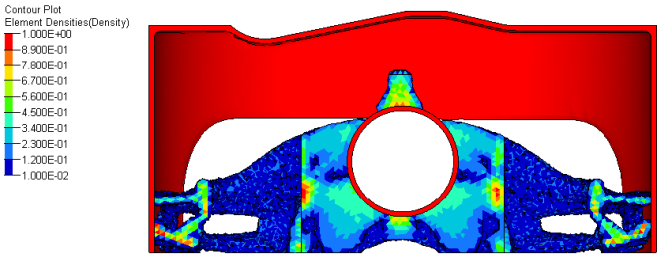

Figure 17. Contour plot PT 0.1 density.

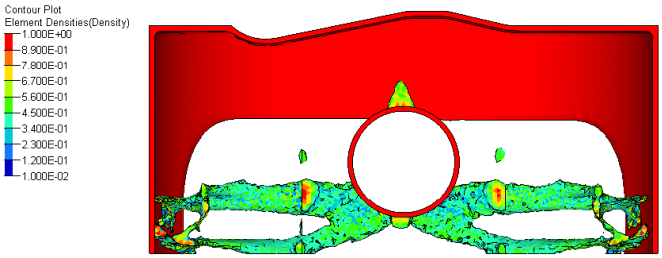

Figure 18. Contour plot PT 0.4 density.

Redesign

The software employed for the piston redesign is Solidworks 2016. The geometry of the piston top, of the ring land, of the pin bosses and of the skirt have not been modified with respect to the original aluminium piston, in order to allow the new steel piston to immediately fit the actual engine, Figure 19. The three different contours plots of Figures 10-15 have been interpreted and the main structural features from each load case have been identified. In particular, the geometries under the crown and below the pin bosses (highlighted with blue in Figure 20) have been designed following the topology optimization results of TDCC and TDCI. The material linking the skirt and the pin bosses (highlighted with yellow in Figure 19) have been design tracing the optimization results corresponding to the piston thrust force load case.

The optimization analysis produced a geometry abundant of small fillets. These features have been implemented accurately in a first steel piston proposal, Figure 21. These geometries (highlighted in Figure 21) produced excessively high values of stress. Therefore, greater radius have been used and a slightly heavier component has been obtained. Using a greater value of the MINDIM parameter has been thought to obtain a clearer solution without small fillets. Unfortunately, this expedient has been useless: a contour plot rich of low density elements has been obtained without provide an effective guide to the design process.

The new steel piston has a mass of 415 g. If compared to the original aluminium piston (380 g), a limited increase of 9% is registered.

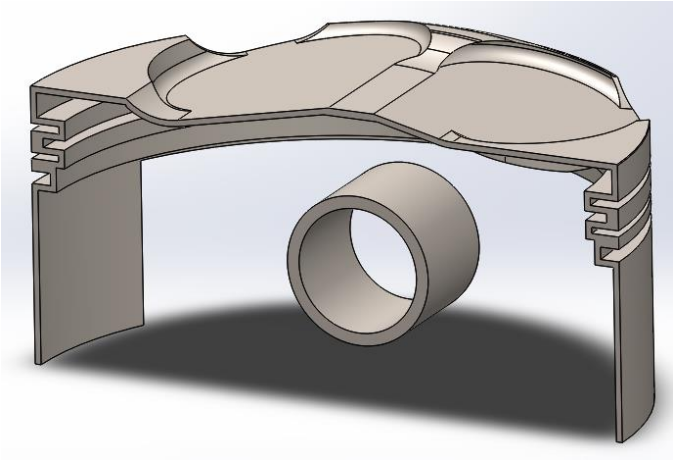

Figure 19. The geometrical boundaries of the piston.

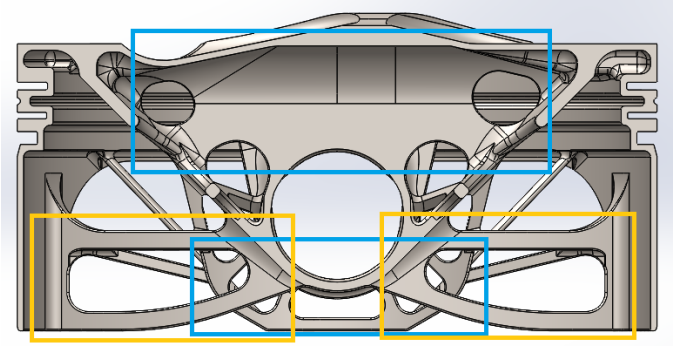

Figure 20. The steel piston.

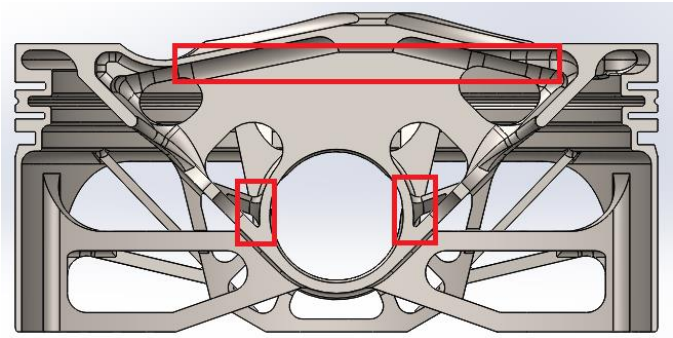

Figure 21. A first proposal of the steel piston, small fillets are highlighted.

Finite Element validation

Several Finite Elements analyses, quite similar to the ones prepared for the aluminium piston, have been performed to validate the designed geometry. The software employed is Marc2013.1. The components involved in the crank mechanism (piston, piston pin and the connecting rod small end) have been discretized and a symmetry plane has been properly used. Figure 22 shows the model employed to mimic the TDCC and TDCI conditions. Figure 23 shows the model employed to mimic the maximum piston thrust force condition. In this case, the connecting rod has been correctly tilted and a rigid surface has been introduced in order to simulate the cylinder liner reaction. About 1.4 million elements have been employed: 260 thousand pentahedral elements (bilinear, 6 nodes, 6 Gaussian integration points), 47 thousand hexahedral elements (bilinear, 8 nodes, 8 Gaussian integration points) and 1.1 million tetrahedral elements (first order, 4 nodes, one Gaussian integration points), the average element size being 0.5 millimetre. The material considered for the analysis of the whole crank mechanism is a generic steel, Table 2.

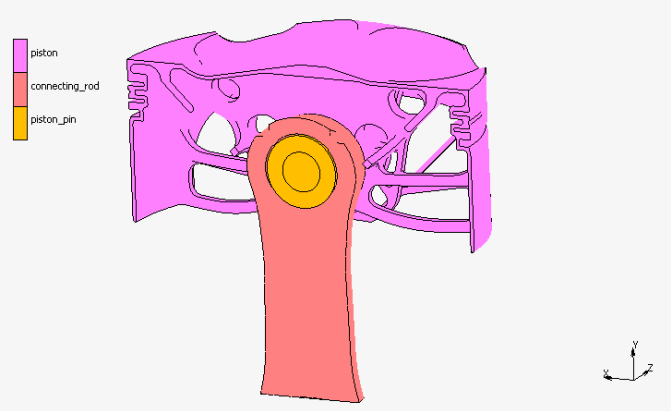

Figure 22. FE model used in the load cases of TDCC and TDCI.

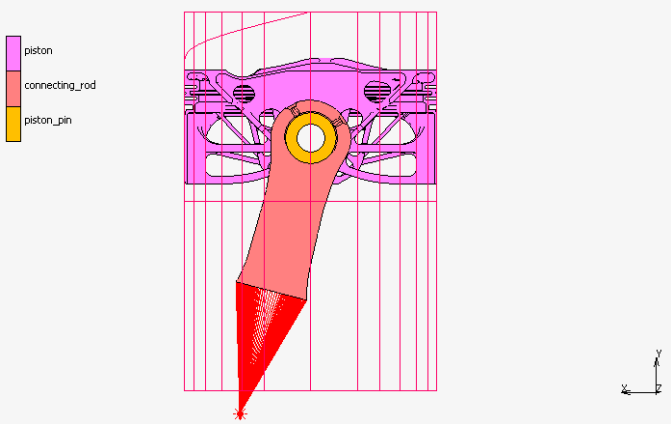

Figure 23. The FE model used for the load case of PT.

Structural analysis

Static and buckle mode models have been set up for each load case.

Top dead centre during combustion (TDCC)

At TDCC a pressure of about 9.1 MPa has been applied on the piston top and a gravity load of 48769 m/s^2 has been assigned to the whole crank mechanism. Fig. 24 displays the von Mises stress contour plot. The material distribution computed by the topology optimization correctly supports the external loads. A maximum value of 385 MPa is registered on the diagonal beams linking the external areas of the top to the pin bosses.
Figure 25 shows the buckle model results. The most critical beam of the wireframe structure collapse with a combustion pressure of about 800 MPa, 88 times greater than the load actually applied by the gas combustion.

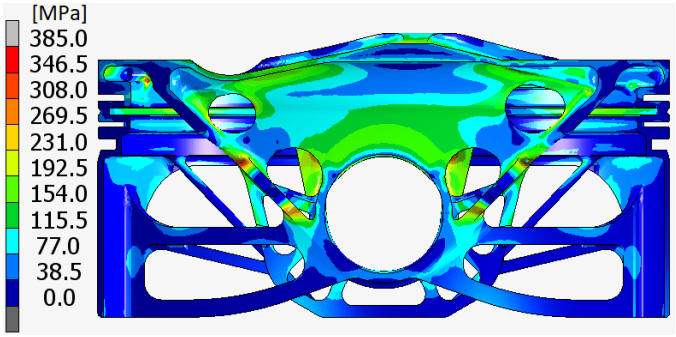

Figure 24. TDCC von Mises contour plot.

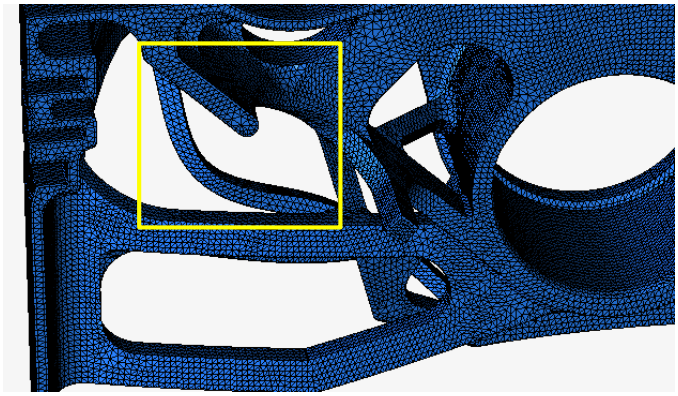

Figure 25. TDCC buckling collapse.

Top dead centre at the beginning of induction stroke (TDCI)

At TDCI a pressure of about 0.07 MPa has been applied on the piston top and a gravity load of 56008 m/s^2 has been assigned to the whole crank mechanism. Figure 26 displays the von Mises stress contour plot. The piston exhibits a lower level of stress if compared to the TDCC case. A maximum value of 320 MPa is registered on the diagonal beams linking the external areas of the top to the pin bosses. The analysis also returns that the buckle mode collapse will be triggered only by a negative acceleration. This result can be easily understood considering that at TDCI, the thinnest beams of the structure are subjected to a tensile load.

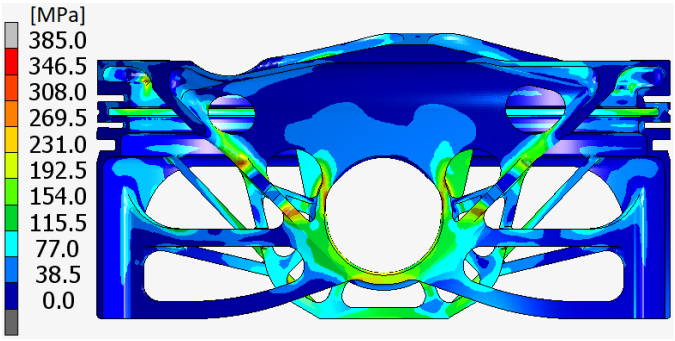

Figure 26. TDCI von Mises contour plot.

Maximum piston thrust force (PT)

At PT a pressure of about 0.8 MPa has been applied on the piston top and a negative gravity load of 22955 m/s^2 has been assigned to the whole crank mechanism. In this load case, the contact interaction between the piston and the liner is crucial. Figure 27 displays the von Mises stress contour plot. A maximum value of 300 MPa is registered on the material linking the skirt to the pin bosses.
Figure 28 shows the buckle model results. The most critical beam of this wireframe structure collapse with a contact normal force 1000 times greater than the load actually applied to the piston. The buckling mode results show that the piston is not subjected to Eulerian instability.

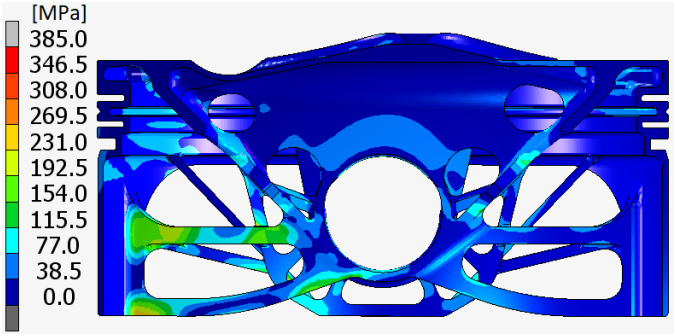

Figure 27.von Mises contour plot.

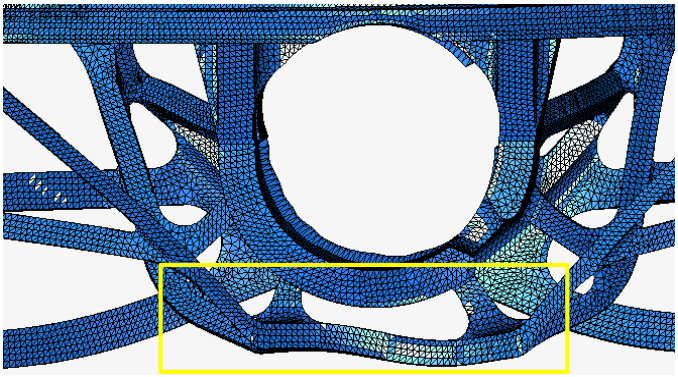
Figure 28. PT buckling collapse.

Fatigue analysis

A fatigue analysis has been performed, based on Dang Van criterion [17, 18]. This is a stress-based multi-axial criterion employed to compute a fatigue safety factor by taking into account a certain load history. A fatigue limit of 400 MPa has been considered. Figure 29 shows the Dang Van safety factor contour plot. The whole component presents a minimum factor greater than one. The most critical areas are restricted and placed on the diagonal beams linking the external areas of the piston top to the pin bosses.

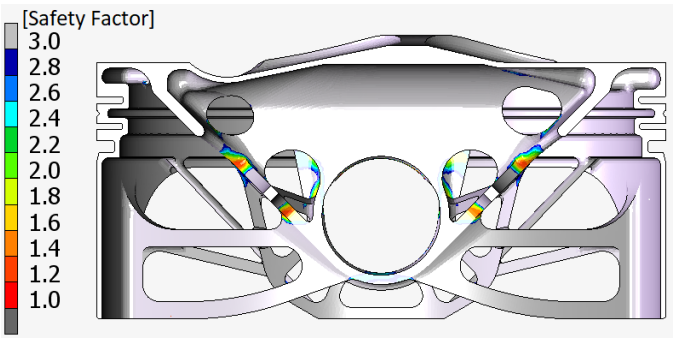

Figure 29. Dang Van safety factor contour plot.

Thermal analysis

A thermal model has been prepared, based on the same boundary conditions of Table 4. In particular, the thermal exchange contribution given by the oil jet and the rest of the splashed oil has been considered to be exactly the same of the previously investigated aluminium piston.

Results

Figure 30 shows the temperature contour plot. The piston crown reaches a maximum temperature of 490°C.
In particular, these high values of temperature are confined to a small angular portion of the valve pocket peripheries, while the rest of the top surface exhibits a comparable temperature distribution with respect to the aluminium piston (ranging from 250°C to 290°C). Such a result has been obtained properly designing very thin geometrical features of the piston top (Figure 31), thus minimizing the thermal resistance through the piston top thickness. In fact, the thermal conductivity of steel can be up to five times lower than the aluminium one. Unfortunately, it has not been possible to remove material under the identified critical portions of the valve pockets periphery without modifying the non-design space (Figure 32). A smoother temperature gradient could be obtained softening the geometry of these keen-edged features, but it will simultaneously increase the combustion chamber volume, thus reducing the compression ratio and the maximum power of the engine. Cooling galleries could be designed in order not to modify the geometry of the crown. Furthermore, an integrated in-cylinder/CHT analysis should be performed in order to guide the redesign process and to predict possible abnormal combustion occurrence related to these concentrated peaks of temperature [19].

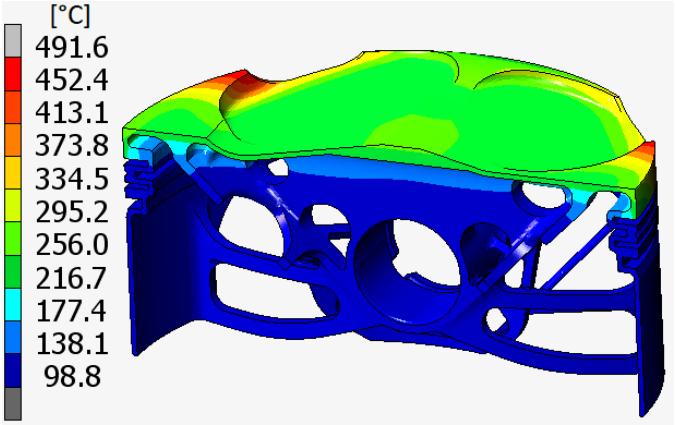

Figure 30. Temperature contour plot.

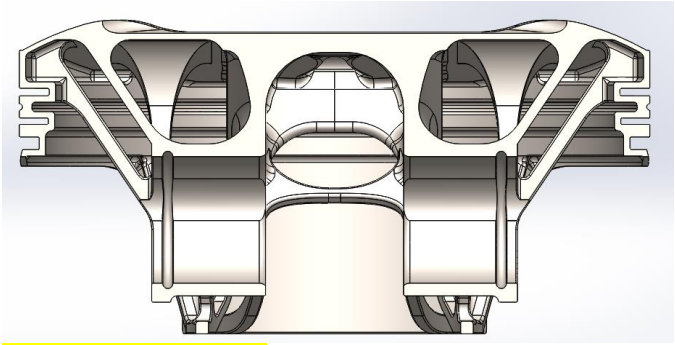
Figure 31. Steel piston section.

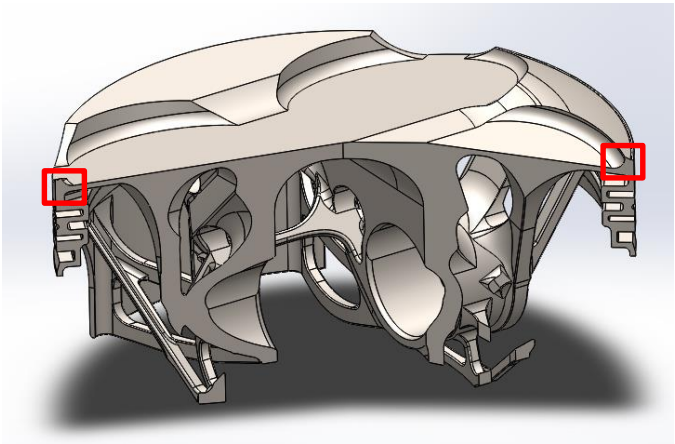
Figure 32. Details of the peripheries of the valve pockets.

Conclusions

A method for a computer aided steel piston design has been proposed. In particular, the presented methodology aimed at finding more efficient layout solutions for the piston framework feasible with Additive Manufacturing techniques. The authors employed topology optimizations to define the optimal structural topology. Special care has to be taken in setting up the optimization process since the choice of the constraints, i.e. the performance targets, of the mesh size and quality and of the optimization parameters directly affect the outcome of the process. The topology optimization results have guided the redesign process towards a wireframe structure abundant of small fillets. The structural analysis have revealed high values of von Mises stress in localized areas, thus larger radius fillets have been adopted. The fatigue analysis underlined the need to review the geometry of the diagonal beams linking the external areas of the piston top to the pin bosses. Preliminary thermal analyses have shown the requirement to modify the geometry of the piston top in order to remove/reduce concentrated peaks of temperatures arising at sharped geometrical features inherited from the original aluminium piston configuration. Such a modification has to be guided by ad hoc integrated in-cylinder/CHT analysis necessary to avoid undesired and detrimental abnormal (knocking) combustion processes that may arise. The new steel piston exhibits a mass of 415 g. If compared to the original aluminium piston (380 g), a limited increase of 9% is registered. The new steel piston could allow high mechanical and thermal loadings to be reached; therefore a wider redesign of the engine components will be necessary in order to totally take advantage of the steel piston adoption.

References

1. M. Giacopini, S. Sissa, R. Rosi, S. Fantoni. “Influence of different temperature distributions on the fatigue life of a motorcycle piston.” Proceedings of the Institution of Mechanical Engineers, Part D: Journal of Automobile Engineering. 229 (9) (2015) 1276-1288, doi:10.1177/0954407014560201.
2. S. Sissa, M. Giacopini, R. Rosi. “Low-cycle thermal fatigue and high-cycle vibration fatigue life estimation of a diesel engine exhaust manifold.” Procedia Engineering. 74 (2014) 105-112, doi:10.1016/j.proeng.2014.06.233.
3. S. Fontanesi, M. Giacopini. “Multiphase CFD-CHT optimization of the cooling jacket and FEM analysis of the engine head of a V6 diesel engine.” Applied Thermal Engineering, 52 (2) (2013) 293-303, doi:10.1016/j.applthermaleng.2012.12.005.
4. K. Schreer, I. Roth, S. Schneider, H. Ehnis. “Analysis of aluminium and steel pistons – Comparison of friction, piston temperature and combustion.” Journal of Engineering for Gas Turbines and Power. 136 (2014) 101506-1, doi:10.1115/1.4027275.
5. M.P. Bendsøe, N. Kikuchi. “Generating optimal topologies in structural design using a homogenization method. Computer methods in applied mechanics and engineering.” 71 (1988) 197-224, doi: 10.1016/0045-7825(88)90086-2.
6. F. Du, Z. Tao. “Study on lightweight of the engine piston based on topology optimization”. Advanced Materials Research. 201-203 (2011) 1308-1311, doi:10.4028/www.scientific.net/AMR.201-203.1308.
7. J. Zhao, F. Du, W. Yao. “Structural analysis and topology optimization of a bent-bar-frame piston based on the variable density approach.” ASME 2014 Dynamic Systems and Control Conference, doi: 10.1115/DSCC2014-6118.
8. D. Brackett, I. Ashcroft, R. Hague. “Topology optimization for additive manufacturing.” Proceedings of the Solid Freeform Fabrication Symposium. (2011) 348–362.
9. S.G. Barbieri, M. Giacopini, V. Mangeruga, S. Mantovani. “A design strategy based on topology optimization techniques for ad additive manufacture high performance engine piston.” Procedia Manufacturing. 11 (2017) 641-649, doi:10.1016/j.promfg.2017.07.162.
10. I. Tolosa, F. Garciandìa, F. Zubiri, F. Zapirain, A. Esnaola. “Study of mechanical properties of AISI 316 stainless steel processed by “selective laser melting”, following different manufacturing strategies.” Int J Adv Manuf Technol. 51 (2010) 639-647, doi: 10.1007/s00170-010-2631-5.
11. A.B. Spierings, T.L. Starr, K. Wegener. “Fatigue performance of additive manufactured metallic parts.” Rapid Prototyping Journal. 19 (2013) 88-94, doi:10.1108/13552541311302932.

12. J. P. Kruth, L. Froyen, J. Van Vaerenbergh, P. Mercelis, M. Rombouts, B. Lauwers. “Selective laser melting of iron-based powder.” Journal of Materials Processing Technology 149 (2004) 616–622, doi:10.1016/j.jmatprotec.2003.11.051.
13. F. J. Kahlen, A. Kar. “Similarity Parameters for Rapid Manufacturing.” Journal of Manufacturing Science and Engineering. 123 (2001) 38-44, doi:10.1115/1.1286472.
14. N. Gardan, A. Schneider, J. Gardan. “Material and process characterization for coupling topological optimization to additive manufacturing.” Computer-Aided Design and Applications, 2015, doi: 10.1080/16864360.2015.1059192.
15. G. Woschni. “A Universally Applicable Equation for the Instantaneous Heat Transfer Coefficient in the Internal Combustion Engine.” SAE Technical Paper (1967) 670931, doi:10.4271FF670931.
16. G. Cantore, M. Giacopini, R. Rosi, A. Strozzi, P. Pelloni, C. Forte, M. Achiluzzi, G.M. Bianchi, L. Ceschini, A. Morri. “Validation of a combined CFD/FEM methodology for the evaluation of thermal load acting on aluminium alloy pistons through hardness measurements in inertial combustion engines.” Metallurgical Science and Technology. 29-1 (2011).
17. K. Dang Van, B. Griveau and O. Message. “On a new multiaxial fatigue limit criterion: theory and application.” In MW Brown and KJ Miller (eds) Biaxial and multiaxial fatigue (EGF 3). London: Mechanical Engineering Publications, 1989, pp. 479–496.
18. K. Dang Van, G. Cailletaud, J.F. Flavenot, A. Le Douaron, H.P. Lieurade. “Criterion for high-cycle fatigue failure under multiaxial loading.” In MW Brown and KJ Miller (eds) Biaxial and multiaxial fatigue (EGF 3). London: Mechanical Engineering Publications, 1989, pp. 459–478.
19. S. Fontanesi, G. Cicalese, G. Cantore, A. D'Adamo. "Integrated In-Cylinder/CHT Analysis for the Prediction of Abnormal Combustion Occurrence in Gasoline Engines," SAE Technical Paper 2014-01-1151, 2014, doi:10.4271/2014-01-1151.